metals

MDPI

Article

Microstructure, Mechanical Properties and Wear Behavior of the Rheoformed 2024 Aluminum Matrix Composite Component Reinforced by Al_2O_3 Nanoparticles

Jufu Jiang [1,*], Guanfei Xiao [1], Changjie Che [1] and Ying Wang [2]

[1] School of Materials Science and Engineering, Harbin Institute of Technology, Harbin 150001, China; guanfeixiao@163.com (G.X.); 18092233726@163.com (C.C.)

[2] School of Mechatronics Engineering, Harbin Institute of Technology, Harbin 150001, China; wangying1002@hit.edu.cn

* Correspondence: jiangjufu@hit.edu.cn; Tel.: +86-187-4601-3176

Received: 3 May 2018; Accepted: 14 June 2018; Published: 15 June 2018

Abstract: The 2024 nanocomposite reinforced with Al_2O_3 nanoparticles was fabricated by the ultrasonic assisted semisolid stirring (UASS) method and rheoformed into a cylinder component. Microstructure, mechanical properties, and wear behavior of the rheoformed composite components were investigated. The results showed that the composite components with complete filling status and a good surface were rheoformed successfully. The deformation of semisolid slurries was mainly dominated by flow of liquid incorporating solid grains (FLS), sliding between solid grains (SSG), and plastic deformation of solid grains (PDS). Mechanical properties of the rheoformed composite components were influenced by stirring temperature, stirring time, and volume fraction of Al_2O_3 nanoparticles. The optimal ultimate tensile strength (UTS) of 358 MPa and YS of 245 MPa were obtained at the bottom of the rheoformed composite components after a 25-min stirring of composite semisolid slurry with 5% Al_2O_3 nanoparticles at 620 °C. Enhancement of mechanical properties was attributed to high density dislocations and dislocation tangles and uniform dispersed Al_2O_3 nanoparticles in the aluminum matrix. Natural ageing led to the occurrence of needle-like Al_2CuMg phase and short-rod-like Al_2Cu phase. UTS of 417 MPa and YS of 328 MPa of the rheoformed composite components were achieved after T6 heat treatment. Improvement of mechanical properties is due to the more precipitated needle-like Al_2CuMg phase and short-rod-like Al_2Cu phase. Wear resistance of the rheoformed composite components was higher than that of the rheoformed matrix component. Wear resistance of the rheoformed composite component increased with an increase in Al_2O_3 nanoparticles from 1% to 7%. A slight decrease in wear rate resulted from 10% Al_2O_3 nanoparticles due to greater agglomeration of Al_2O_3 nanoparticles. A combination mechanism of adhesion and delamination was determined according to worn surface morphology.

Keywords: 2024 aluminum matrix composites; rheoformed; Al_2O_3 nanoparticles; microstructure; mechanical properties

1. Introduction

Metal matrix composites (MMC) have exhibited some obvious advantages such as high specific strength, high specific stiffness, and good wear resistance [1–3]. Fabrication technology of MMC involves stirring casting [4,5], powder metallurgy [6–8], squeeze casting [9–11], and semisolid stirring [12–14]. In addition, selective laser melting (SLM) was employed to fabricate high-performance alloys and MMC [15–17]. As a typical MMC, aluminum matrix composite reinforced by ceramic

particles (AMCCP) also exhibited some important applications in the automotive and aerospace industries [18,19]. The reinforced ceramic particles are composed of micro-sized ceramic particles and nano-sized ceramic particles. In recent years, aluminum matrix composites reinforced with nano-sized ceramic particles (AMCNCP) have attracted researchers' attention because of higher strength, increased dimensional stability, high thermal stability, high modulus, and good wear resistance as compared to conventional materials [20]. Raju et al. [21] evaluated fatigue of nano-sized Al_2O_{3p}/2024 composite and found that it was slightly increased as compared to matrix material. Raturi et al. [22] reported mechanical, tribological, and micro structural behavior of the Al 7075 matrix reinforced with nano Al_2O_3 particles and concluded that tensile, impact, and flexural strength of the composite were enhanced as compared with the matrix alloy. Sajjadi et al. [23] investigated the fabrication and mechanical properties of A356 composite reinforced with micro and nano-sized Al_2O_3 particles by a developed compocasting method. The results showed that the hardness of the composites increased with increasing particle weight fraction and decreasing particle size.

However, it is very difficult to disperse uniformly nano-sized ceramic particles in the matrix alloy due to higher surface energy and specific surface area as compared to micro-sized ceramic particles. Therefore, some novel methods were developed to realize uniform dispersion of nano-sized ceramic particles such as Al_2O_3 and SiC. For example, uniform dispersion of Al_2O_3 nanoparticles in matrix alloy was achieved successfully via incorporating milled powders of Al_2O_3 nanoparticles and aluminum or copper into A356 alloy melt [24,25]. Acoustic streaming and cavitation created by ultrasonic wave led to a uniform dispersion of nano-sized SiC particles in molten A356 aluminum alloy [26,27]. Semisolid stirring and ultrasonic wave were joined together to obtain a uniform dispersion of nano-sized SiC particles in 7075 aluminum matrix. It was attributed to the controllable viscosity of semisolid slurries and acoustic streaming and cavitation created by ultrasonic wave [28].

Matrix materials of AMCNCP mainly have been focused on A356 [24–27], 7075 [28], A357 [29], and 6061 [8] aluminum alloys, but 2024 matrix material has not been studied in detail. The present investigation will deal with microstructure and mechanical properties of 2024 aluminum matrix composite reinforced with Al_2O_3 nanoparticles.

2. Materials and Methods

2.1. Fabrication of 2024 Aluminum Matrix Composite Reinforced with Al_2O_3 Nanoparticles

Commercial 2024 aluminum alloy was used as matrix material. Its chemical composition was determined via an Axios pw4400 X-ray fluorescence spectrometer and contained 4.52 wt % Cu, 1.51 wt % Mg, 0.56 wt % Mn, 0.18 Si wt %, 0.12 wt % Fe, 0.02 wt % Zn, and a balance of Al. α-Al_2O_3 nanoparticles with an average size of 60 nm were used as reinforcement of the composite. Solidus temperature of 529 °C and liquidus temperature of 650 °C were achieved from a differential scanning calorimetry (DSC) test. Figure 1 gives a schematic diagram of fabrication and rheoforming of 2024 matrix composite semisolid slurry. As shown in Figure 1, there were three main procedures in the fabrication and rheoforming of composite semisolid slurry. In the first procedure, α-Al_2O_3 nanoparticles with an average size of 60 nm parceled by pure aluminum foil were added into the melt after 2024 aluminum alloy was melted at 670 °C and held for 20 min. The XRD pattern of as-received Al_2O_3 nanoparticles shows the presence of α-Al_2O_3 peaks (Figure 2). The melt with α-Al_2O_3 nanoparticles was treated for 10 min via an ultrasonic device. In the second procedure, melt with α-Al_2O_3 nanoparticles was stirred and cooled to the predefined semisolid temperature, and then isothermally stirred for the required time, as shown in Table 1.

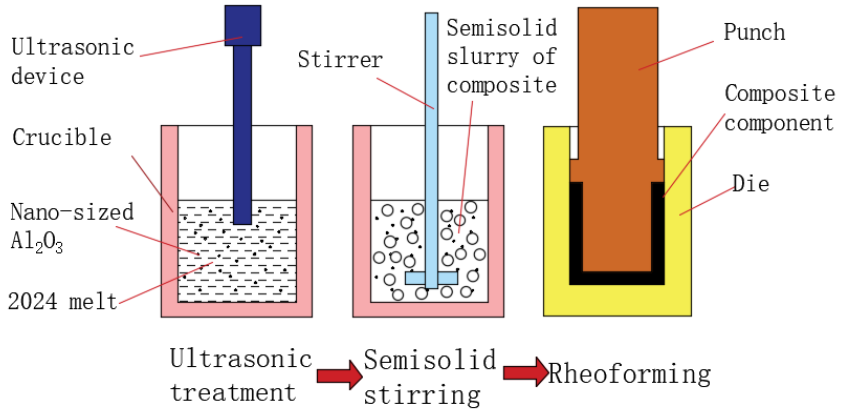

Figure 1. Schematic diagram of fabricating and rheoforming the semisolid slurry of composite.

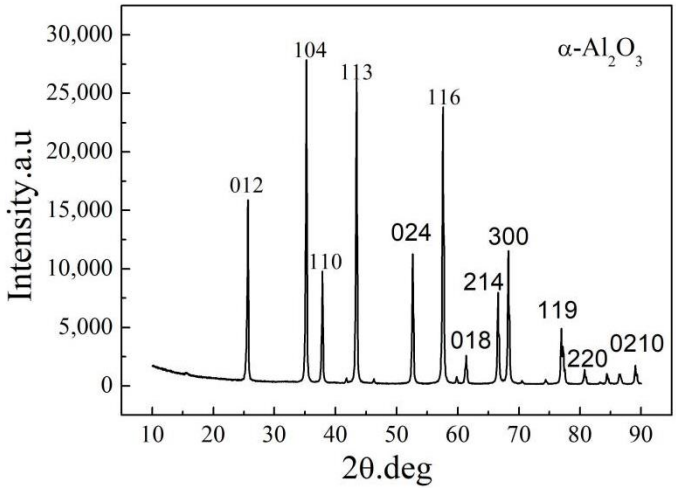

Figure 2. XRD pattern of as-received Al_2O_3 nanoparticles.

Table 1. Experimental scheme of the rheoformed 2024 aluminum matrix composite reinforced by Al_2O_3 nanoparticles and original 2024 components.

Serial Number	Stirring Time (Min)	Stirring Temperature (°C)	Al_2O_3 Volume Fraction (%)	Ultrasonic Treatment Time (Min)	Force (kN)	Dwell Time (s)	Preheated Temperature of Die (°C)
1	5	620	5	10	2000	20	400
2	10	620	5	10	2000	20	400
3	15	620	5	10	2000	20	400
5	20	620	5	10	2000	20	400
6	25	620	5	10	2000	20	400
7	30	620	5	10	2000	20	400
8	25	610	5	10	2000	20	400
9	25	615	5	10	2000	20	400
10	25	625	5	10	2000	20	400
11	25	630	5	10	2000	20	400
12	25	620	0	10	2000	20	400
13	25	620	1	10	2000	20	400
14	25	620	3	10	2000	20	400
15	25	620	7	10	2000	20	400
16	25	620	10	10	2000	20	400
17	25	610	0	10	2000	20	400
18	25	615	0	10	2000	20	400
19	25	625	0	10	2000	20	400
20	25	630	0	10	2000	20	400

In the third procedure, the fabricated semisolid slurries of the composite were carried directly into the die cavity with a preheated temperature of 400 °C and rheoformed (i.e., semisolid slurry was directly formed into the final part under some pressure) under a force of 2000 kN. The detailed

experimental scheme was shown in Table 1. Two composite components under the same process parameters were rheoformed in order to improve the accuracy of tensile test. Therefore, thirty composite components were rheoformed successfully. Ten original 2024 components without Al_2O_3 nanoparticles were also rheoformed in order to compare microstructure, mechanical properties, and wear behavior with composite components.

2.2. Microstructure Observation and Measurement of Mechanical and Wear Properties

The microstructural specimens cut from composite components were firstly ground with 200, 400, 600, 800, 1200, and 2000 grit papers and then polished with 0.1 μm diamond paste. The specimens were etched for about 10 s by Keller's reagent (4 mL HF, 6 mL HCL, 8 mL HNO3 and 82 mL water) and observed by using Olympus GX71 optical microscope (OM, Olympus Coporation, Toyko, Japan), Quanta 200 FEG scanning electron microscope (SEM, FEI, Hillsboro, OR, USA), and talos f200x transmission electron microscopy (TEM, FEI, Hillsboro, OR, USA) equipped with an energy dispersive X-ray spectrometer (EDX). Transmission electron microscopy specimens were fabricated via cutting 1 mm slices from the rheoformed composite component with a wire cutting machine, and then mechanically ground to a thickness of 100 μm. Then 3 mm diameter disks were cut from the thin slices by punching. Ion milling was carried out on these 3 mm diameter disks.

Tensile specimens cut from composite components were machined into standard tensile specimens according to ASTM Standard Test Methods for Tension Testing of Metallic Materials, E8M [30]. The sampled location and drawing of tensile specimens were indicated in Figure 3. Eight specimens were obtained from side wall of the two rheoformed composite components under the same process parameters and four specimens were obtained from the bottom. Four side-wall tensile specimens and two bottom specimens were directly carried out on tensile test at room temperature. The other four side-wall specimens and two bottom specimens were firstly treated via T6 heat treatment involving the solution treatment for 2 h at 490 °C and ageing for 10 h at 190 °C and then used as a tensile test at room temperature. The tensile strength of the side wall reported in this paper was obtained from the average value of data of four side-wall specimens. The tensile strength of bottom was achieved from the average value of data of two bottom specimens. The dry sliding wear tests were carried out on a pin-on-disc wear-testing apparatus. The disc was made from 5Cr15 steel. After the rheoformed matrix and composite components were formed, they were machined into the samples with dimensions of $\phi 6 \times 15$ mm for the dry sliding wear tests. The process parameters of wear test involved a distance of 1000 m, a speed of 0.8 m/s, and a load of 30 N.

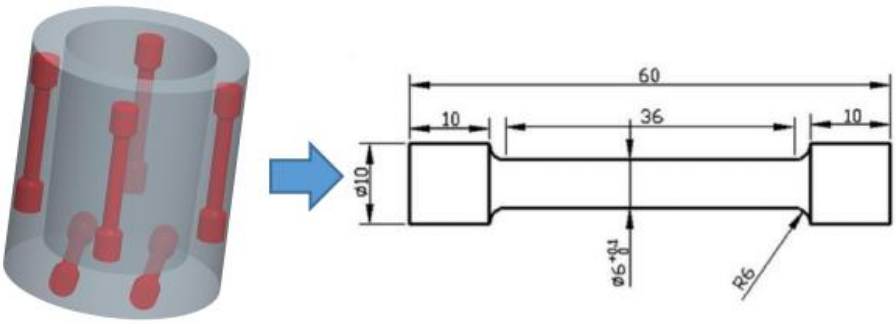

Figure 3. Sampled location and drawing of tensile specimens.

3. Results and Discussion

3.1. Macrograph and Microstructure of the Rheoformed Composite Component

Figure 4 presented the whole and half-sectional macrographs of the rheoformed composite component reinforced by 5 vol % Al_2O_3 nanoparticles at 620 °C and for 25 min stirring time.

As shown in Figure 4a, complete filling status and good surface quality were obtained from the rheoformed composite component. No obvious porosity and incomplete filling status were found in the half-sectional macrograph of the rheoformed composite component (Figure 4b). It illustrates that densified microstructure was obtained in the rheoformed composite components. The densified microstructure is beneficial to improve the mechancial properties of the rheoformed composite components. In order to characterize the microstructure and mechanical properties in different locations of the rheformed composite components, the microstructural specimens were achieved from the locations A to D (Figure 4b), and tensile specimens were obtained from the side wall and bottom (Figure 3).

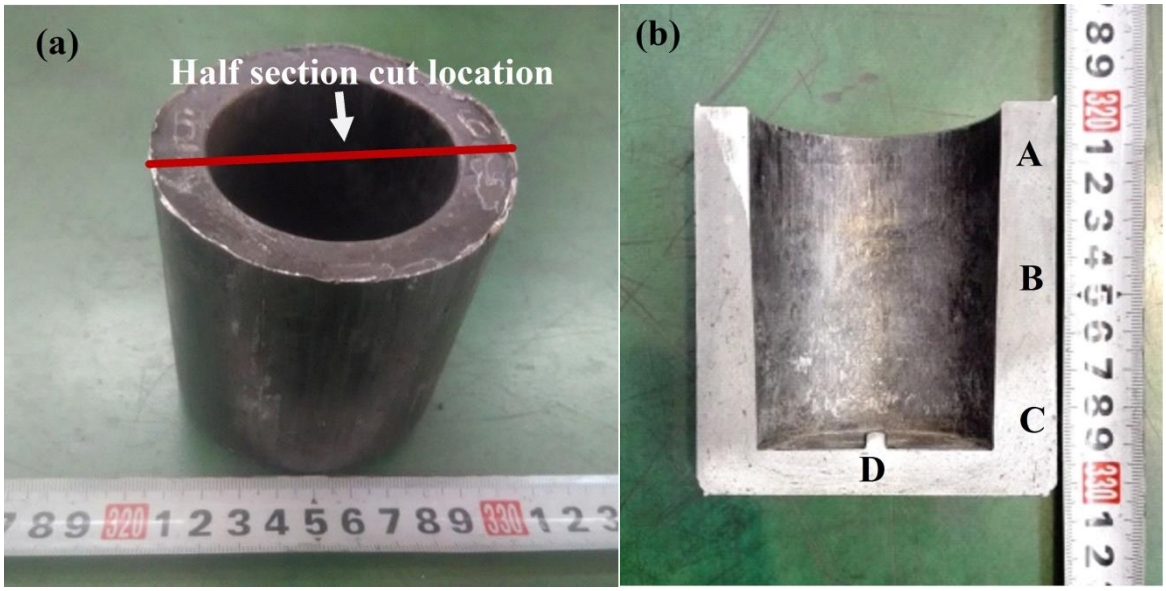

Figure 4. Whole and half-sectional macrographs of rheoformed 2024 aluminum matrix composite component reinforced by 5 vol % Al_2O_3 nanoparticles at 620 °C and for 25 min stirring time (**a**) whole macrograph; (**b**) half-sectional macrograph.

Microstructure in different locations of the rheoformed composite components is shown in Figure 5. As indicated in Figure 5a,b, microstructure in locations A and B consisted of near spheroidal grains and liquid phase. It illustrates that no obvious plastic deformation occurred in the solid grains in locations A and B during the rheoforming process. The microstructure in locations C and D consisted of elongated solid grains and liquid phase (Figure 5c,d). It indicates that obvious plastic deformation along flowing direction of semisolid slurries occurred in the solid grains in locations C and D. There are four deformation mechanisms in the semisolid processing, liquid flow (LF), flow of liquid incorporating solid grains (FLS), sliding between solid grains (SSG), and plastic deformation of solid grains (PDS) [31]. When the semisolid slurry was rheoformed in the die cavity, it showed a backward extrusion mode. The flow front of the semisolid slurry in locations A and B is a free surface [27], indicating the lowest resistance to flow. The flow velocity of liquid phase is higher than that of solid phase. It led to more liquid phase existed in locations A and B. As a consequence, deformation compatibility of liquid phase is higher than that of semisolid slurry in locations C and D. Therefore, deformation in locations A and B depends on flow of liquid incorporating solid grains (FLS) and sliding between solid grains (SSG).

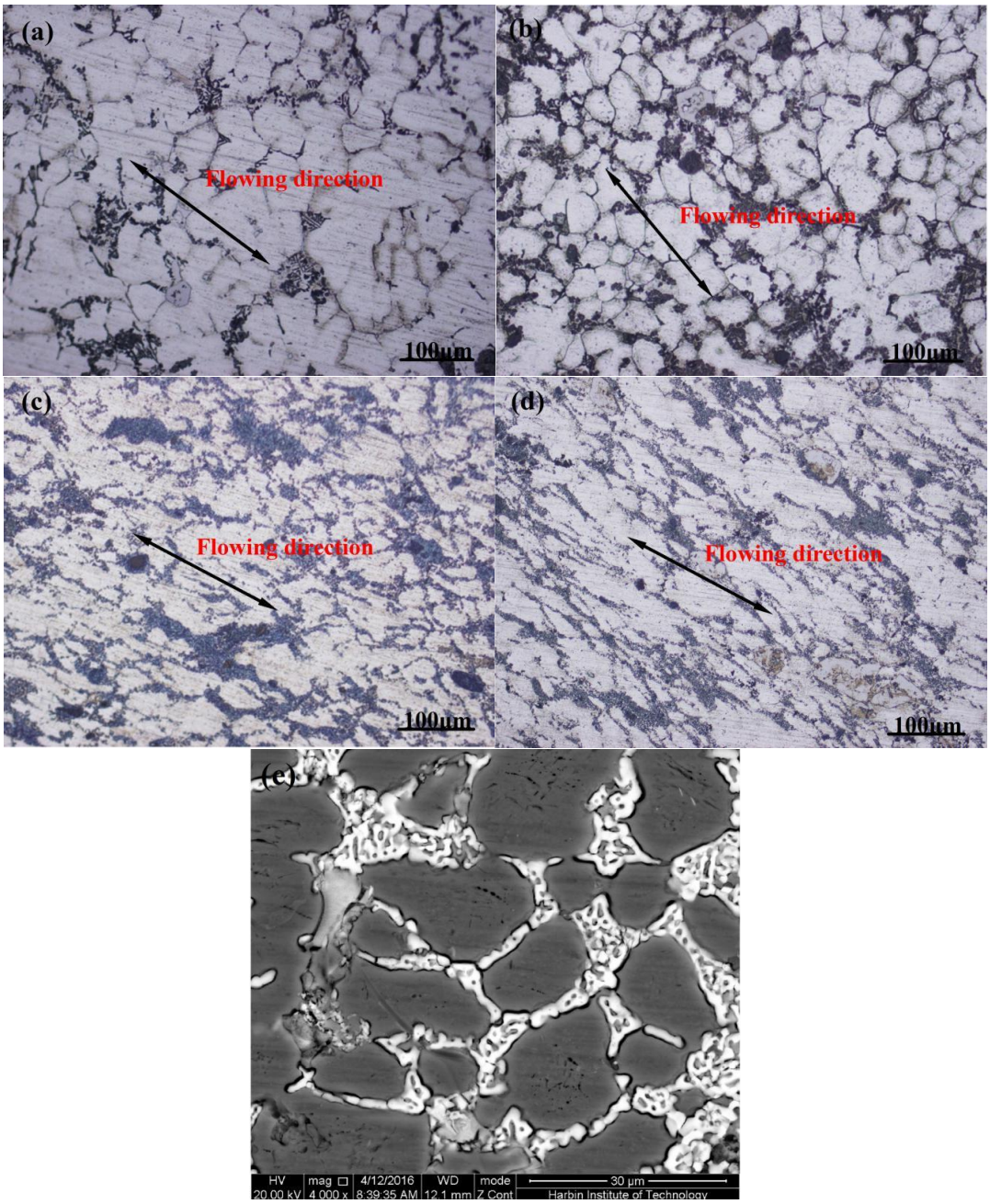

Figure 5. Microstructure of 2024 aluminum matrix composite component reinforced by 5 vol % Al_2O_3 nanoparticles rheoformed at 620 °C and for 25 min stirring time. (**a**) Optical microscope (OM) image in location A of the composite component; (**b**) OM image in location B of the composite component; (**c**) OM image in location C of the composite component; (**d**) OM image in location D of the composite component; (**e**) SEM image in location B of the composite component.

It led to near spheroidal solid grains with no obvious plastic deformation. However, the deformation in locations C and D was mainly dominated by plastic deformation of solid grains (PDS). Consequently, the elongated solid grains were created along the flowing direction. In addition, it can be noted that the deformation degree in location D is higher than that in location C due to low fraction liquid. Figure 5e shows the SEM image of the rheoformed composite component. It illustrates further that the microstructure in location B consisted of near spheroidal grains due to dependence of the deformation on FLS and SSG.

The microstructure in various locations of the rheoformed original 2024 is similar to that of the composite component (Figure 6). As a consequence, the deformation mechanisms in locations A and B rely on FLS and SSG. The deformation mechanisms in locations C and D depend on PDS. The SEM image in location B of 2024 matrix component is presented in Figure 6e. As shown in Figure 6e, similar to the composite, the microstructure of the rheoformed original 2024 consisted of near spheroidal grains and liquid phase. It illustrates that the deformation mechanism depends on the FLS and SSG. However, the size of the solid grains of the rheoformed composite component is obviously smaller than that of the rheoformed original 2024. It was attributed to the action of nano-sized Al_2O_3 particles as heterogeneous nuclei during the solidification of aluminum alloy [24].

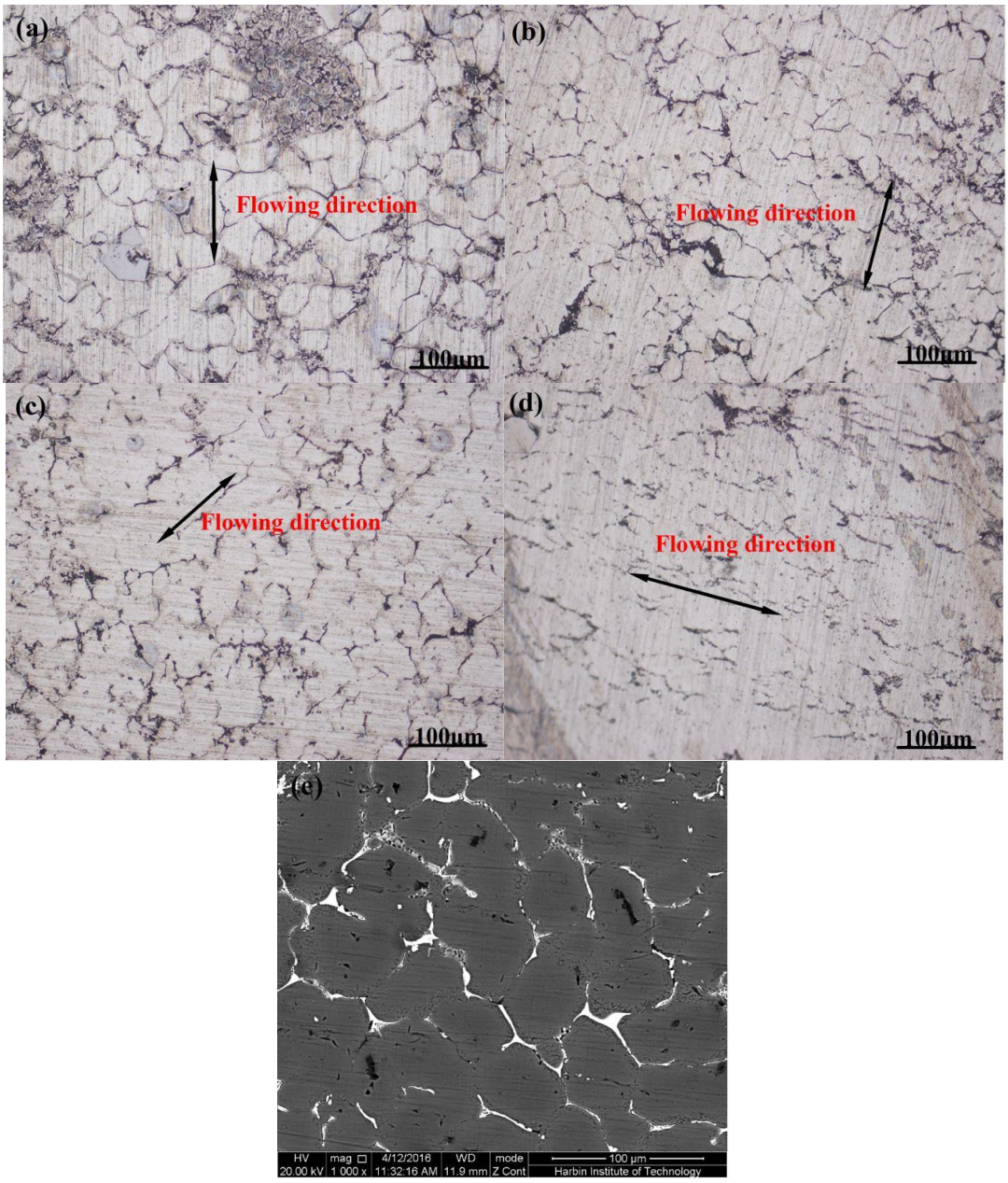

Figure 6. Microstructure of the original 2024 rheoformed at 620 °C and for 25 min stirring time. (**a**) OM image in location A of the matrix component; (**b**) OM image in location B of the matrix component; (**c**) OM image in location C of the matrix component; (**d**) OM image in location D of the matrix component; (**e**) SEM image in location B of 2024 matrix component.

3.2. Influence of Stirring Temperature and Stirring Time on Mechanical Properties

Figure 7 shows mechanical properties of the rheoformed composite components reinforced by 5 vol % Al_2O_3 nanoparticles and matrix components for 25 min stirring time at different stirring temperatures. As indicated in Figure 7, ultimate tensile strength (UTS), yield strength (YS), and elongation all increase and then decrease with an elevated stirring temperature. The highest UTS of 315 MPa in the side wall and the highest UTS of 358 MPa at the bottom were obtained at 620 °C. The highest YS of 238 MPa in the side wall and the highest YS of 245 MPa at the bottom were obtained at 620 °C. The highest elongation of 5.3% in the side wall and the highest elongation of 5.6% at the bottom were all obtained at 620 °C. Similar to the composite components, the optimal mechanical properties were also obtained at 620 °C. It illustrated that 620 °C was the optimal stirring temperature to obtain the highest mechanical properties. In addition, UTS and elongation at the bottom were higher than the side wall. It is due to the fact that severe plastic deformation occurred in the bottom location of the rheoformed composite components (Figure 4d). The UTS and YS of the matrix components are lower than those of the composite components. The YS in the side wall of the composite and matrix components was close to that at the bottom.

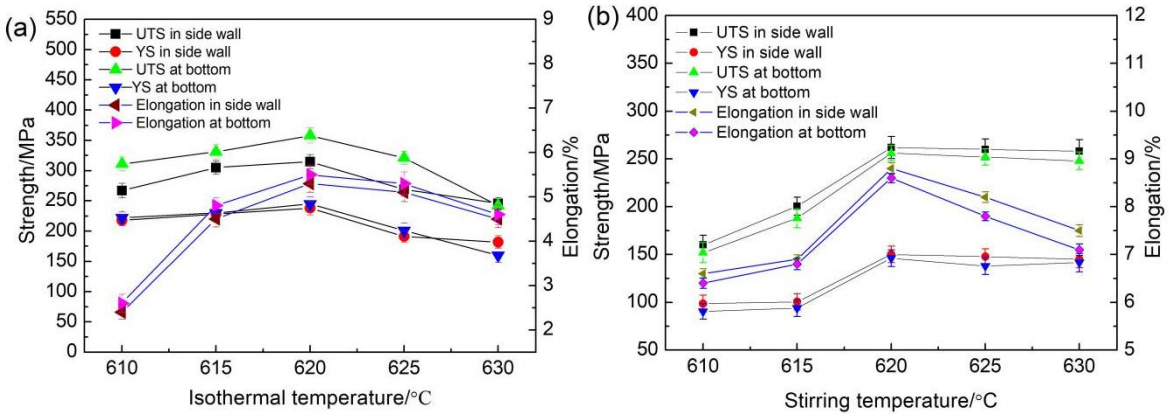

Figure 7. Influence of different stirring temperature on mechanical properties of rheoformed composite components reinforced by 5 vol % Al_2O_3 nanoparticles for 25 min stirring time and matrix components (**a**) composite components; (**b**) matrix components.

Microstructure evolution with elevating stirring temperature was given in Figure 8. The microstructure specimens were cut from location B as shown in Figure 4b. The microstructure consisted of near spheroidal solid grains and liquid phase due to dependence of deformation mechanism on FLS and SSG. Low stirring temperature leads to coarse spheroidal grains. Even some obvious dendrites were found in the microstructure of the rheoformed composite parts. It has an adverse influence on the mechanical properties of the rheoformed composite parts. With the increase in stirring temperature, the grain size of spheroidal grains decreased. The average grain sizes obtained from image analysis are 57 μm, 76 μm, 47 μm, 55 μm, and 54 μm respectively when the stirring temperatures are 610 °C, 615 °C, 620 °C, 625 °C, and 630 °C.

Therefore, the average size of solid grains in the microstructure at 620 °C is obviously smaller than those at other stirring temperatures. According to the Hall-Petch effect [31], fine grains can lead to an increase in YS and UTS. Furthermore, stirring temperatures higher than 625 °C lead to aggregation of liquid phase, which is detrimental to mechanical properties. When stirring temperature is higher than 625 °C, more aggregation of liquid phase also reduced controllable viscosity of semisolid slurries due to the lack of solid grains. The dispersion effect of Al_2O_3 nanoparticles was reduced due to decreased viscosity of semisolid slurries. As a result, greater agglomeration of Al_2O_3 nanoparticles occurred in the microstructure, leading to a decrease in mechanical properties of the rheoformed composite components.

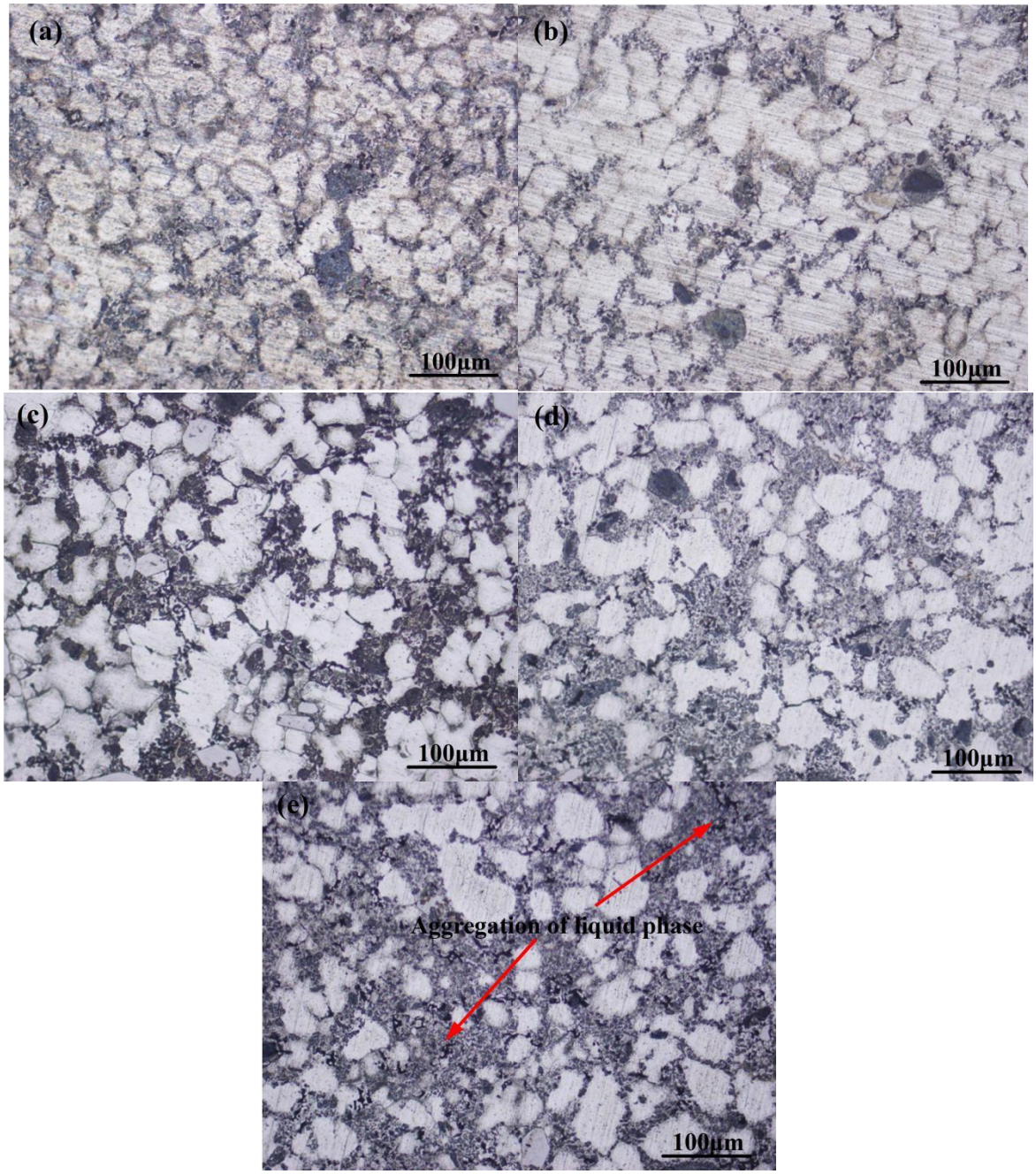

Figure 8. OM microstructure in location B of rheoformed 2024 aluminum matrix composite component reinforced by 5 vol % Al_2O_3 nanoparticles for 25 min stirring time at various stirring temperatures (**a**) 610 °C; (**b**) 615 °C; (**c**) 620 °C; (**d**) 625 °C; (**e**) 630 °C.

Figure 9 shows mechanical properties of the rheoformed composite component reinforced by 5 vol % Al_2O_3 nanoparticles at 620 °C for different stirring times. As shown in Figure 7, mechanical properties of rheoformed composite components increased significantly when stirring time increased from 5 min to 25 min. Mechanical properties of the rheoformed composite component changed slightly when stirring time increased from 25 min to 30 min. Similar results were found in the rheoformed cylindrical part of the 7075 aluminum matrix composite reinforced with nano-sized SiC particles [28]. The highest mechanical properties including UTS of 358 MPa, YS of 245 MPa, and elongation of 5.6%

were achieved at bottom of the rheoformed cylindrical part of the composite reinforced with Al_2O_3 nanoparticles for 25 min stirring time at 620 °C.

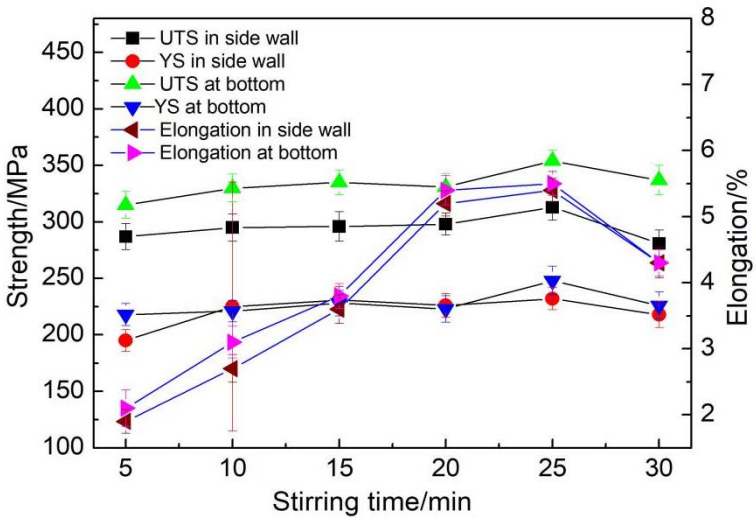

Figure 9. Influence of different stirring time on mechanical properties of rheoformed 2024 aluminum matrix composite component reinforced by 5 vol % Al_2O_3 nanoparticles at 620 °C.

Increasing stirring time resulted in a fine-grained microstructure of composite semisolid slurries (Figure 10). As indicated in Figure 10a, coarse solid grains of more than 200 μm were found in the microstructure when stirring time was 5 min. With an increase in stirring time, solid grains were refined significantly (Figure 10b–e). When stirring time was 25 min, the average size of solid grains was about 46 μm. Fine-grained microstructure can improve mechanical properties of the rheoformed composite components due to the Hall-Petch effect [32]. However, the grain size of solid grains changed slightly when stirring time increased from 25 min to 30 min. As a result, the mechanical properties of the rheoformed composite components also changed slightly, or even showed a slight decrease.

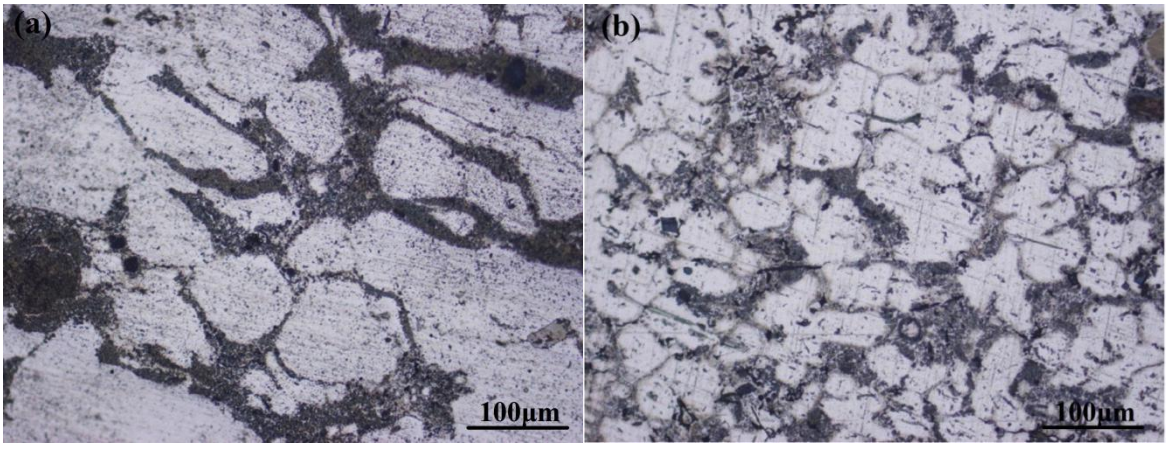

Figure 10. *Cont.*

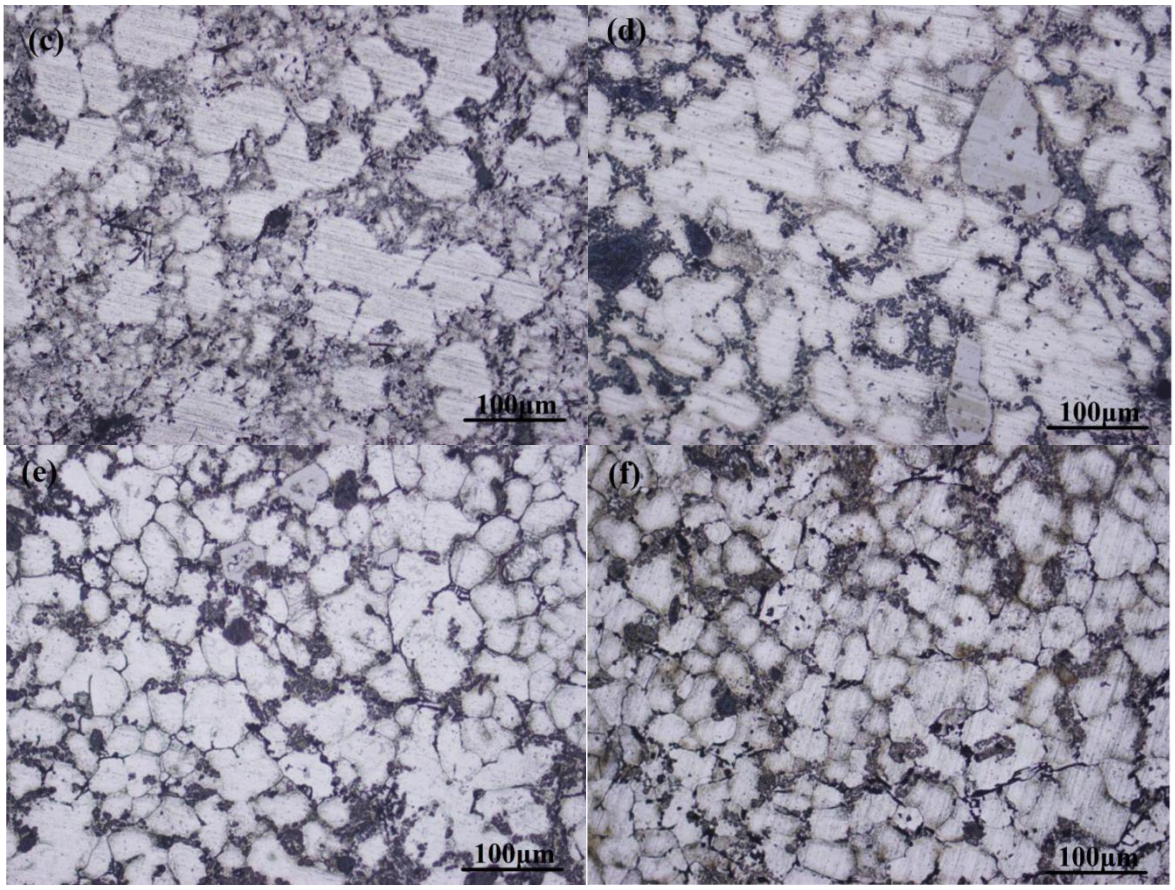

Figure 10. Influence of different stirring time on OM microstructure in location B of the rheoformed 2024 aluminum matrix composite component reinforced by 5 vol % Al_2O_3 nanoparticles at 620 °C (**a**) 5 min; (**b**) 10 min; (**c**) 15 min; (**d**) 20 min; (**e**) 25 min; (**f**) 30 min.

3.3. Influence of Volume Fraction of Al_2O_3 Nanoparticles on Mechanical Properties

Figure 11 shows the influence of volume fraction of Al_2O_3 nanoparticles on mechanical properties of the rheoformed composite components. As indicated in Figure 11, UTS and YS of the rheoformed composite components increased when the volume fraction of Al_2O_3 nanoparticles increased from 0 to 5%. UTS values in the side wall and at the bottom of the matrix components are 268 MPa and 272 MPa respectively. When the volume fraction of Al_2O_3 nanoparticles increased to 5%, they reached 315 MPa and 358 MPa respectively. The increasing degrees of UTS and YS are 17.5% and 31.7% respectively. Al_2O_3 nanoparticles act as barriers of dislocations mobility, leading to an improvement of UTS and YS [33]. In addition, mismatch of coefficient of thermal expansion (CTE) between the matrix and reinforcement phase, load transfer from matrix to reinforcement phase and Orowan strengthening mechanism also play an important role in improving the mechanical properties [34–36]. Al_2O_3 nanoparticles also acted as heterogeneous nuclei for the aluminum alloy matrix, leading to a grain-refined strengthening effect [24,37,38]. The improvement of mechanical properties may be related to the residual stress and fracture toughness at the interface between the Al_2O_3 and the Al matrix. However, it is very difficult to measure the residual stress and fracture toughness at the interface between the Al_2O_3 and the Al matrix, and it could be helpful to employ nanoindentation and pillar splitting techniques as reported by Matteo Ghidelli et al. [39,40].

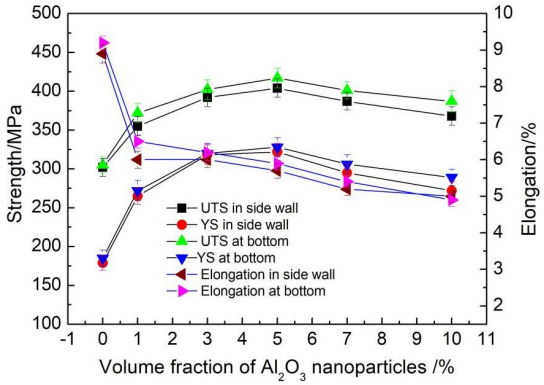

Figure 11. Influence of volume fraction of nano-sized Al_2O_3 on mechanical properties of rheoformed 2024 aluminum matrix composite component reinforced by 5 vol % Al_2O_3 nanoparticles at 620 °C for 25 min stirring time.

In addition, it can be noted that UTS and YS of the rheoformed composite components decreased slightly when the volume fraction of Al_2O_3 nanoparticles was more than 5%. It was attributed to greater agglomeration of Al_2O_3 nanoparticles that occurred in the composite due to a large volume fraction of Al_2O_3 nanoparticles [37]. A similar phenomenon was found in the research of Mazahery et al. [41] and Su et al. [37]. Mechanical properties in the present study were higher than those of Su et al. [37]. It may be due to the effect of a different fabrication method and different component shape on mechanical properties. Elongation of the rheoformed composite components is lower than that of the matrix component. In addition, elongation of the rheoformed composite components decreased with increasing volume fraction of Al_2O_3 nanoparticles. UTS at the bottom of the rheoformed composite components was higher as compared to that of the side wall. Figure 12 depicts the microstructure of rheoformed composite reinforced by nano-sized Al_2O_3 particles and matrix components at 620 °C and for 25 min stirring time.

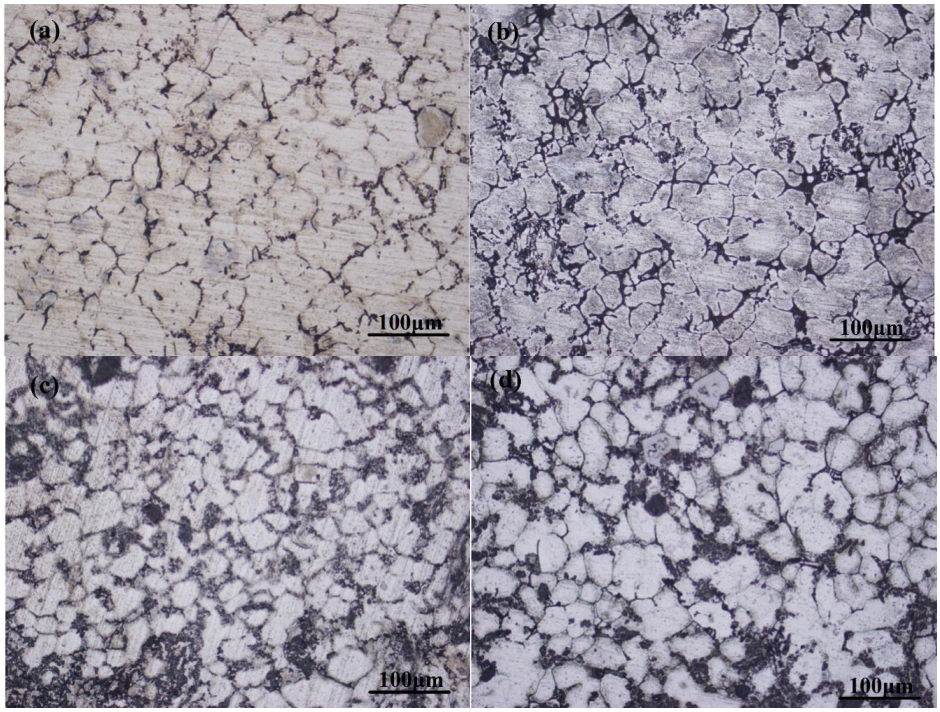

Figure 12. *Cont.*

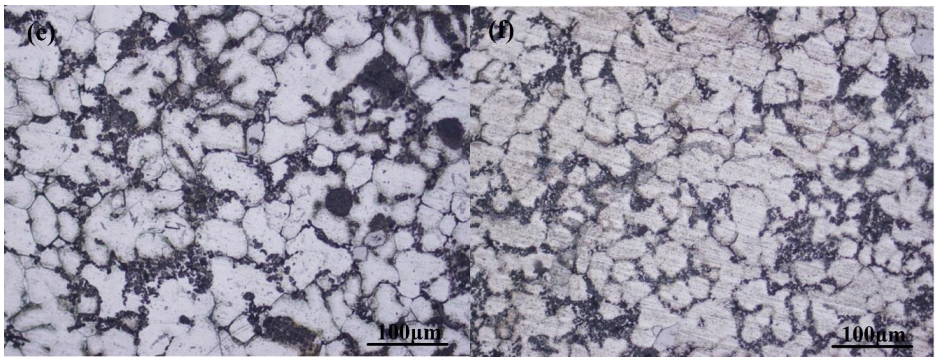

Figure 12. OM microstructure of rheoformed 2024 aluminum matrix composite component reinforced by different volume fraction of Al_2O_3 nanoparticles at 620 °C and for 25 min stirring time (**a**) 2024 matrix; (**b**) 1%; (**c**) 3%; (**d**) 5%; (**e**) 7%; (**f**) 10%.

Average grain size of the rheoformed composite components was smaller than that of the matrix component. It is due to the increasing heterogeneous nucleation for the aluminum matrix created by Al_2O_3 nanoparticles [37,38]. It is helpful to improve the UTS and YS of the rheoformed composite components due to a grain-refined strengthening effect [24,37,38].

3.4. Microstructure Characterization of the Rheoformed Composite Components

Figure 13 shows TEM micrographs at bottom of the rheoformed composite component reinforced by 5 vol % Al_2O_3 nanoparticles. As shown in Figure 13a–e, Al_2O_3 nanoparticles distributed uniformly in the matrix alloy. It is due to the fact that cavitation and acoustic streaming created via ultrasonic wave dispersed Al_2O_3 nanoparticles uniformly [26,42]. In addition, further dispersion of Al_2O_3 nanoparticles was obtained via controllable viscosity of semisolid slurries [27–29]. However, few Al_2O_3 nanoparticles were found in the TEM microstructure at a stirring temperature of 630 °C (Figure 13f). It may be due to the fact that greater agglomeration of Al_2O_3 nanoparticles leads to nonuniform dispersion of Al_2O_3 nanoparticles. This result also provided good evidence for the decreased mechanical properties of the rheoformed composite components at 630 °C (Figure 7a).

High density dislocations and dislocation tangles were found in the TEM images. Deformation of composite semisolid slurries depends on flow of liquid incorporating solid grains (FLS), sliding between solid grains (SSG), and plastic deformation of solid grains (PDS). PDS dominated the deformation of the semisolid slurry at the bottom. Therefore, plastic deformation at the bottom mainly relied on dislocation mobility. As a result, some dislocations were created due to plastic deformation, as shown in Figure 13. Twin crystal was noticed in the TEM microstructure (Figure 13b). It indicated that twinning also occurred in the plastic deformation of solid grains of semisolid slurries. Furthermore, some sub-grains were found in the twin crystal. It is due to the fact that dynamic recovery occurred in rheoformed composite components during the cooling course. Furthermore, Al_2O_3 nanoparticles were surrounded by these high density dislocations (Figure 13a,c,d).

Al_2O_3 nanoparticles acted as barriers of dislocations, leading to an enhancement of the mechanical properties of the rheoformed composite components [33]. It demonstrates that two strengthening mechanisms including dislocation strengthening caused by PDS and interaction between Al_2O_3 nanoparticles and dislocations play an important role in improving the mechanical properties of the rheoformed composite components together.

EDX analysis of Al_2O_3 nanoparticles on microstructure of rheoformed composite components reinforced was shown in Figure 14. Al_2O_3 nanoparticles, Al_2Cu phase, and $MgAl_2O_4$ phase were determined via mapping of Al, Cu, Mg, and O elements.

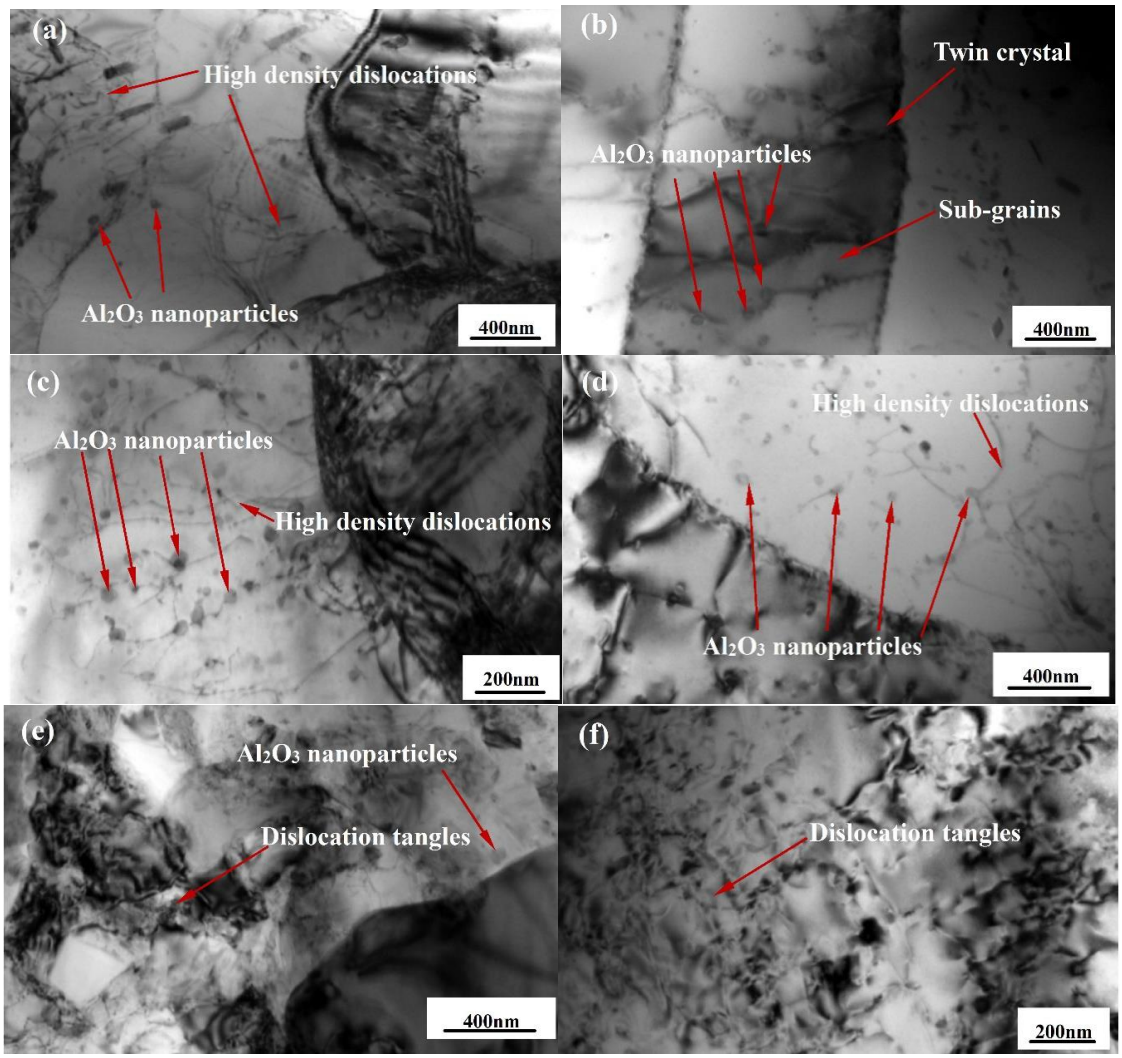

Figure 13. TEM micrographs of rheoformed composite component reinforced by 5 vol % Al_2O_3 nanoparticles at (**a**,**b**) 610 °C; (**c**,**d**) 620 °C and (**e**,**f**) 630 °C.

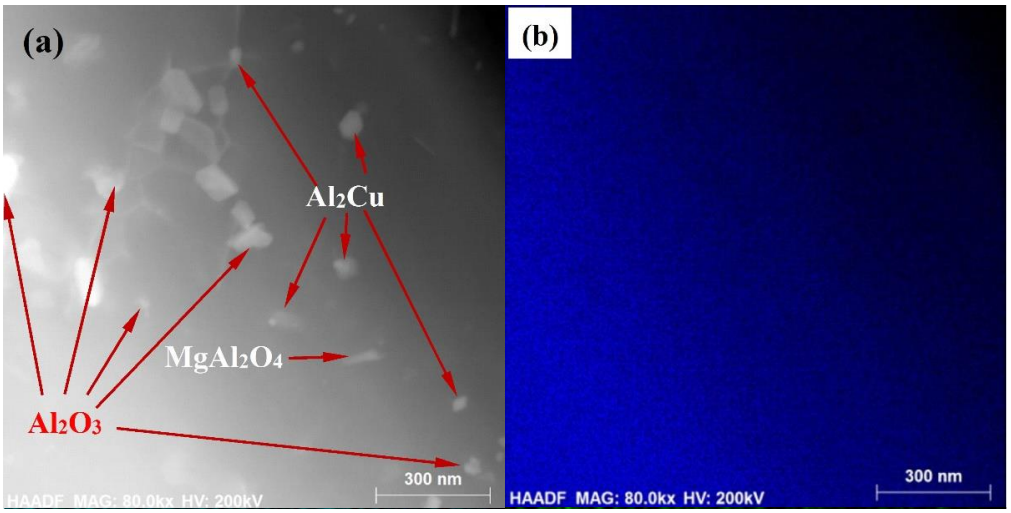

Figure 14. *Cont*.

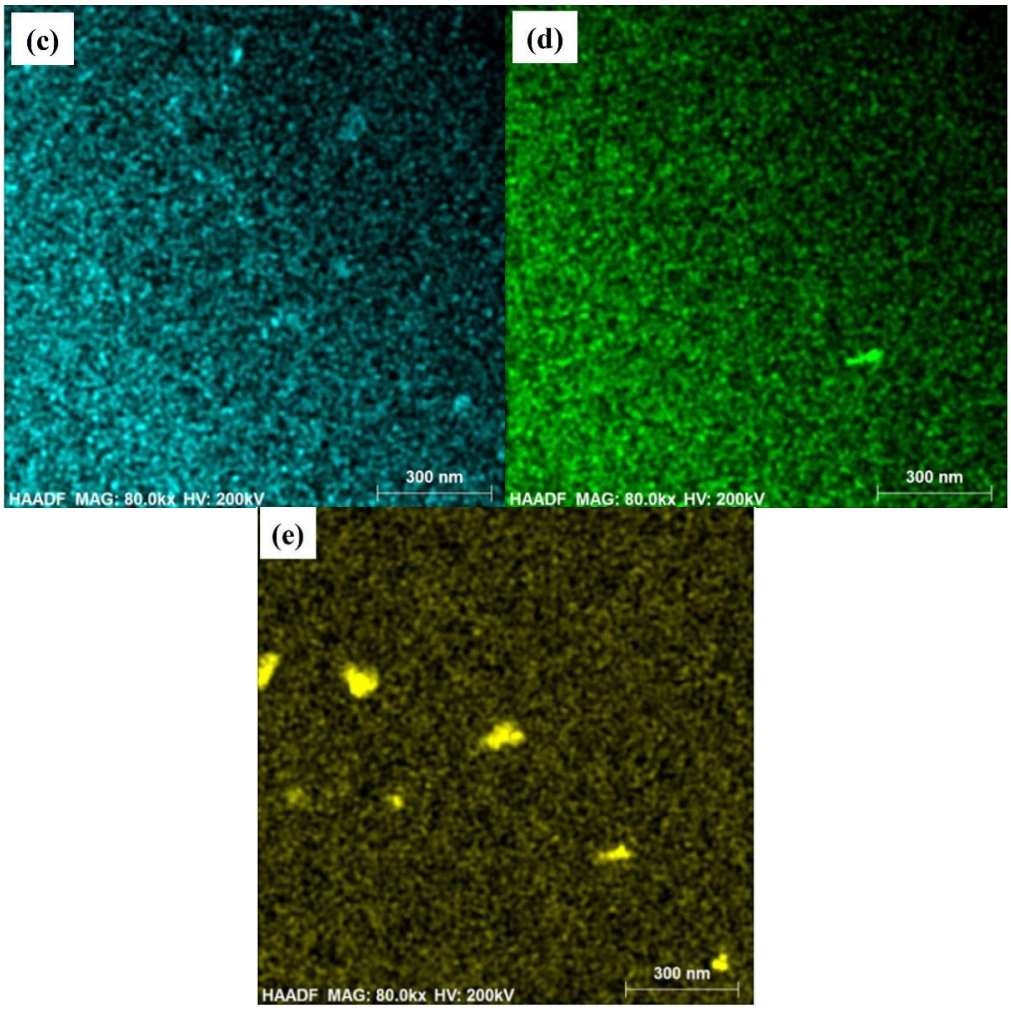

Figure 14. Energy dispersive X-ray spectrometer (EDX) analysis of nano-sized Al_2O_3 on microstructure of rheoformed 2024 aluminum matrix composite component reinforced by 5 vol % Al_2O_3 nanoparticles at 615 °C for for 25 min stirring time (**a**) TEM micrograph; (**b**) Al; (**c**) Cu; (**d**) Mg; (**e**) O.

As indicated in Figure 14, uniform dispersion of Al_2O_3 nanoparticles was noted in the TEM image due to double dispersion of cavitation and acoustic streaming created by ultrasonic wave and controllable viscosity of semisolid slurries. Existence of Al_2Cu phase was due to natural ageing that occurred at room temperature. $MgAl_2O_4$ phase illustrates that an interface reaction occurred in the interface of Al and Al_2O_3 nanoparticles due to existence of Mg element. $MgAl_2O_4$ phase has some advantages such as low density, high melting point, good wear resistance, good heat stability, and high mechanical properties [43,44]. Furthermore, relatively good wetting was obtained at the interface Al, $MgAl_2O_4$, and Al_2O_3 [45]. Therefore, the existence of $MgAl_2O_4$ phase has no effect on mechanical properties of the rheoformed composite components.

Figure 15 shows TEM microstructure and SAED of rheoformed composite components reinforced by 5 vol % Al_2O_3 nanoparticles for 25 min stirring time at 615 °C and 625 °C. As indicated in Figure 15, short-rod-like Al_2Cu phase and needle-like Al_2CuMg phase were determined via selected area electron diffraction (SAED). The second phases such as Al_2Cu phase and Al_2CuMg act as the role of strengthening the 2024 aluminum alloy. After the rheoformed composite components were cooling down to room temperature, these second phases precipitated in the 2024 matrix and strengthened it due to natural ageing that occurred in the components. These second phases also hindered the dislocation movement while the semisolid slurries were deformed. As a result, the mechanical properties of the rheoformed composite component were improved.

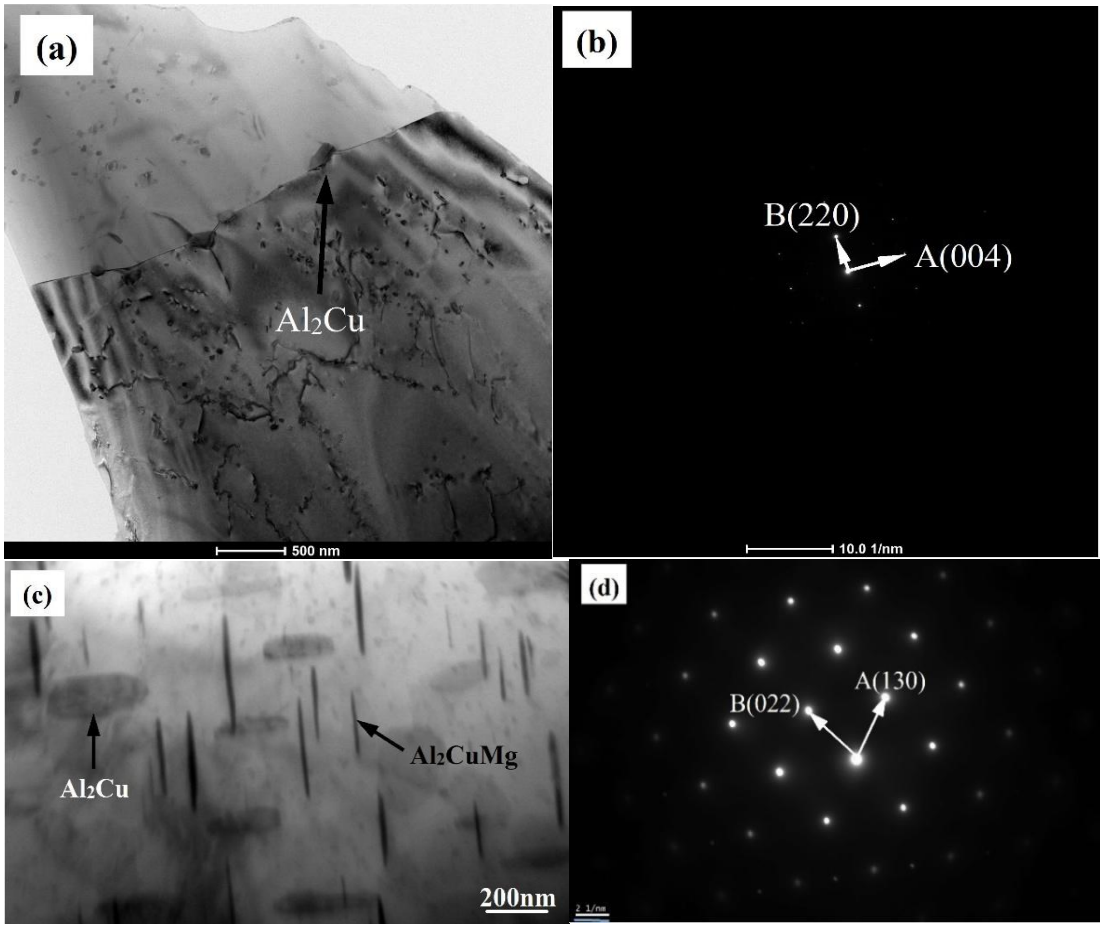

Figure 15. TEM microstructure and selected area electron diffraction (SAED) of rheoformed 2024 aluminum matrix composite component reinforced by 5 vol % Al_2O_3 nanoparticles for 25 min stirring time at 615 °C and 625 °C (**a**) TEM image at 615 °C (**b**) SAED at 615 °C (**c**) TEM image at 625 °C (**d**) SAED at 625 °C.

SEM image and EDX analysis in location B of the rheoformed composite component are presented in Figure 16. As shown in Figure 16a, the microstructure consisted of spheroidal solid grains (grey black color) and liquid phase (white color). It illustrates that the deformation mechanism of semisolid slurry in location B belongs to flow of liquid incorporating solid grains (FLS), sliding between solid grains (SSG). The atom ratio of aluminum and copper at grain boundary is close to 2:1 according to the Figure 16b. It illustrated that the liquid phase at the grain boundary was mainly composed of θ phase (Al_2Cu). The spheroidal solid grains contained a large amount of Al elements and a small amount of Cu and Mg elements, as show in Figure 16c. It illustrates that the spheroidal solid phase is α-Al phase. The α-Al phase is a solid solution of copper and magnesium in aluminum. Existence of O element was attributed to oxidation occurred in the grinding course of the specimens.

3.5. Influence of T6 Heat Treatment on Mechanical Properties

Mechanical properties of the rheoformed composite components reinforced by Al_2O_3 nanoparticles at 620 °C and for 25 min stirring time after T6 heat treatment are indicated in Figure 17. As indicated in Figure 17, mechanical properties of the rheoformed composite components were improved significantly after T6 heat treatment. UTS of 417MPa and YS of 328 MPa were achieved at the bottom of the rheoformed composite components at 620 °C. UTS and YS of the composite components with T6 heat treatment were 16.5% and 20.6% respectively, higher than those of the composite component without T6 heat treatment. Elongation of the composite components with T6

heat treatment was increased by 5.6% as compared to the composite component without T6 heat treatment. UTS and YS of the composite components with T6 heat treatment were increased by 36.7% and 49.1% respectively as compared to the matrix component with T6 heat treatment.

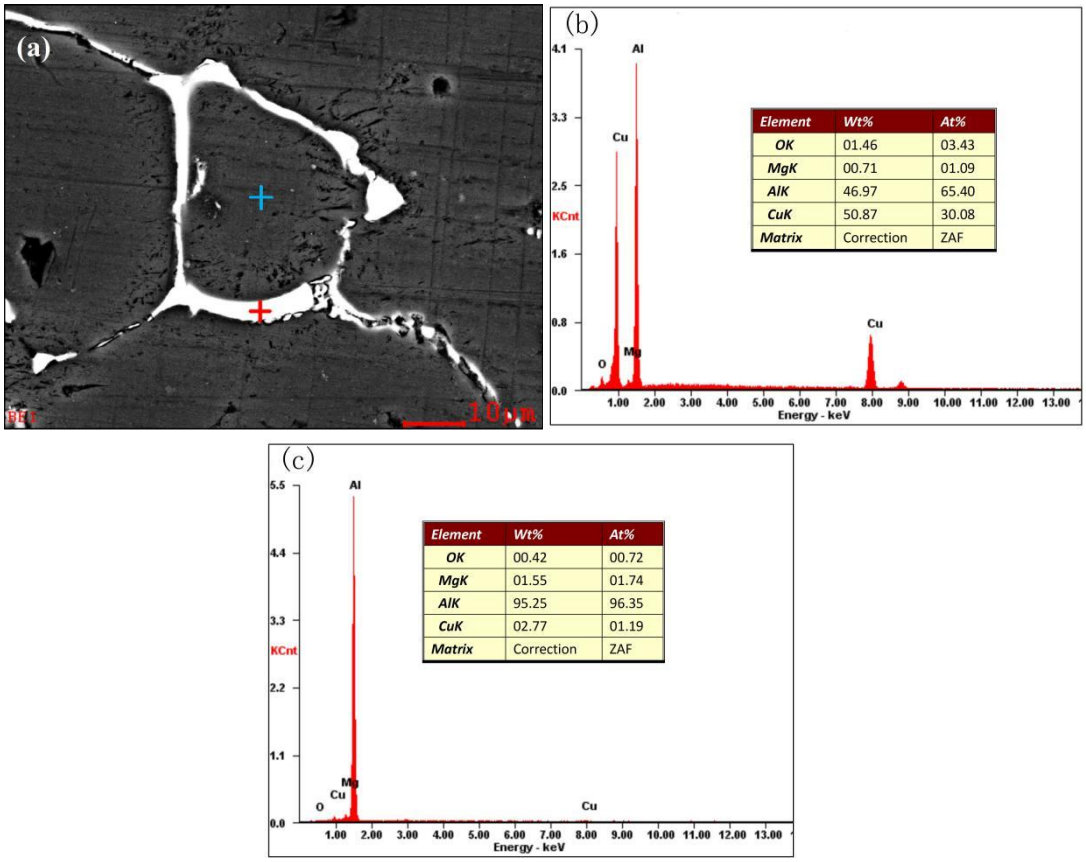

Figure 16. SEM image and EDX analysis of the rheoformed matrix components (**a**) SEM image; (**b**) EDX in location marked with red cross; (**c**) EDX in location marked with blue cross.

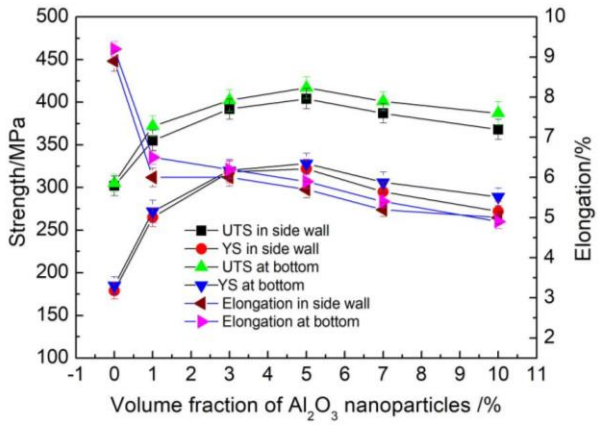

Figure 17. Mechanical properties of rheoformed 2024 aluminum matrix composite component reinforced by Al_2O_3 nanoparticles at 620 °C and for 25 min stirring time after T6 heat treatment.

TEM and EDX of the rheoformed composite components reinforced by 5 vol % Al_2O_3 nanoparticles at 620 °C after T6 heat treatment are shown in Figure 18. Short-rod-like Al_2Cu phase and needle-like Al_2CuMg phase were found in the TEM image of the rheoformed composite components.

The length and width of the short-rod-like Al_2Cu phase are about 100 nm and 65 nm respectively. As for needle-like Al_2CuMg phase, its length varies from 150 nm to 200 nm. Its width is in a range from 20 nm to 50 nm. The mechanical properties of the rheoformed composite component after T6 treatment were improved because of the needle-like Al_2CuMg phase and the short-rod-like Al_2Cu phase.

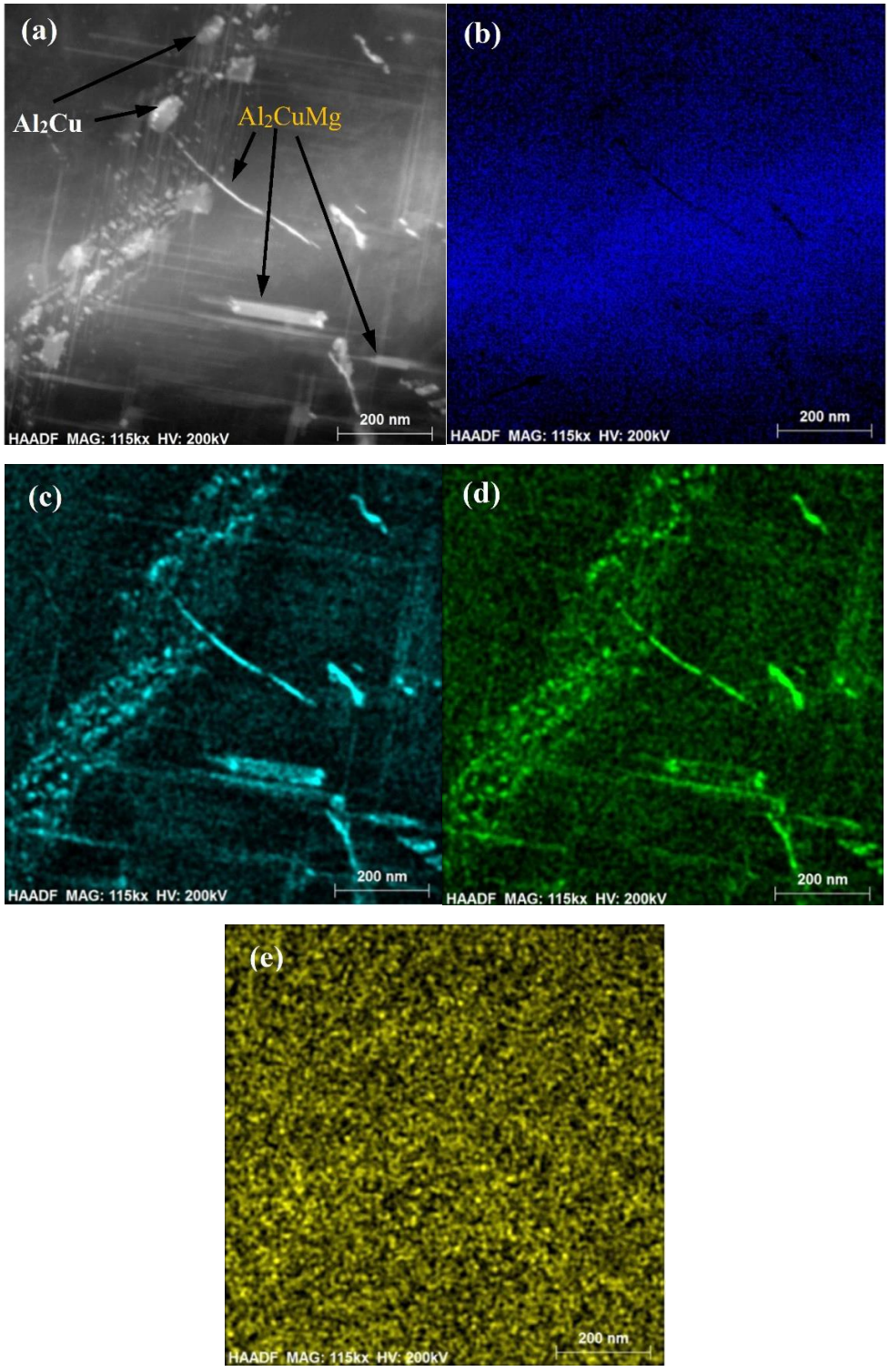

Figure 18. TEM and EDX of rheoformed 2024 aluminum matrix composite component reinforced by 5 vol % Al_2O_3 nanoparticles at 620 °C after T6 heat treatment (**a**) TEM image; (**b**) Al; (**c**) Cu; (**d**) Mg; (**e**) O.

Figure 19 shows the XRD patterns of the rheoformed composite components with T6 and without T6 treatment. The XRD pattern of the rheoformed composite components without T6 showed the presence of the Al peaks, Al_2Cu peaks, and Al_2O_3 peaks.

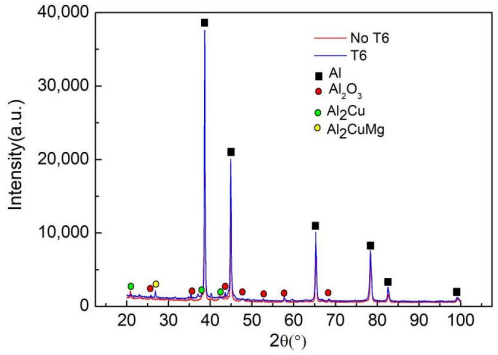

Figure 19. XRD analysis of rheoformed 2024 aluminum matrix composite component reinforced by 5 vol % Al_2O_3 nanoparticles at 620 °C for 25 min stirring time before and after T6 heat treatment.

Al_2CuMg phase besides Al phase, Al_2Cu phase, and Al_2O_3 nanoparticles was also detected in the XRD pattern of the rheoformed composite components with T6. It illustrates that more needle-like Al_2CuMg phase besides short-rod-like Al_2Cu phase precipitated in the rheoformed composite components with T6. As a result, mechanical properties of the rheoformed composite components with T6 were improved significantly as compared to the rheoformed composite components without T6.

3.6. Wear Behavior of the Rheoformed Composite Components

Figure 20 shows wear rate of the rheoformed composite components reinforced by different volume fraction Al_2O_3 nanoparticles at 620 °C for 25 min stirring time. As shown in Figure 20, wear resistance of the rheoformed composite components increased significantly as compared to that of the rheoformed matrix components. Furthermore, wear resistance of the rheoformed composite components increased when volume fraction of Al_2O_3 nanoparticles increased from 1% to 7%. The research of Alhawari et al. [46] also showed that wear resistance of the composite part formed via semisolid processing was higher than that of the composite part via conventional stirring casting. When volume fraction of Al_2O_3 nanoparticles reached 10%, wear rate of the rheoformed composite components decreased slightly as compared to that of the rheoformed composite components with 5% Al_2O_3 nanoparticles. Greater agglomeration of Al_2O_3 nanoparticles leads to difficult uniform dispersion of Al_2O_3 nanoparticles. It led to a decrease in effective dispersion of Al_2O_3 nanoparticles in the 2024 matrix, reducing wear resistance.

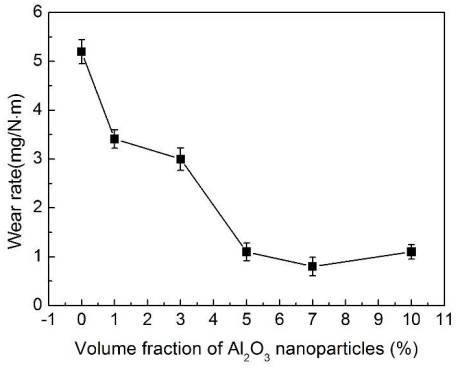

Figure 20. Wear rate of rheoformed 2024 aluminum matrix composite component reinforced by different volume fraction Al_2O_3 nanoparticles at 620 °C for 25 min stirring time.

The specimens subjected to wear test have been examined via SEM (Figure 21). The surface exhibited some clear longitudinal abrasive grooves due to the ploughing effects of harder steel asperities. With an increase of volume fraction of Al_2O_3 nanoparticles, the depth of ploughing grooves became shallow. It indicates that the composite's resistance to wear increases. It is due to the fact that the increase in volume fraction of Al_2O_3 nanoparticles led to an increase in the hardness of the composite. Increase of the hardness of the material is beneficial to improve the resistance to wear [47]. In addition, a delamination was found in the microstructure of the worn surface. It illustrates that the dominant wear mechanism was a combination of adhesion and delamination mechanisms, similar to the findings of Alhawari [46].

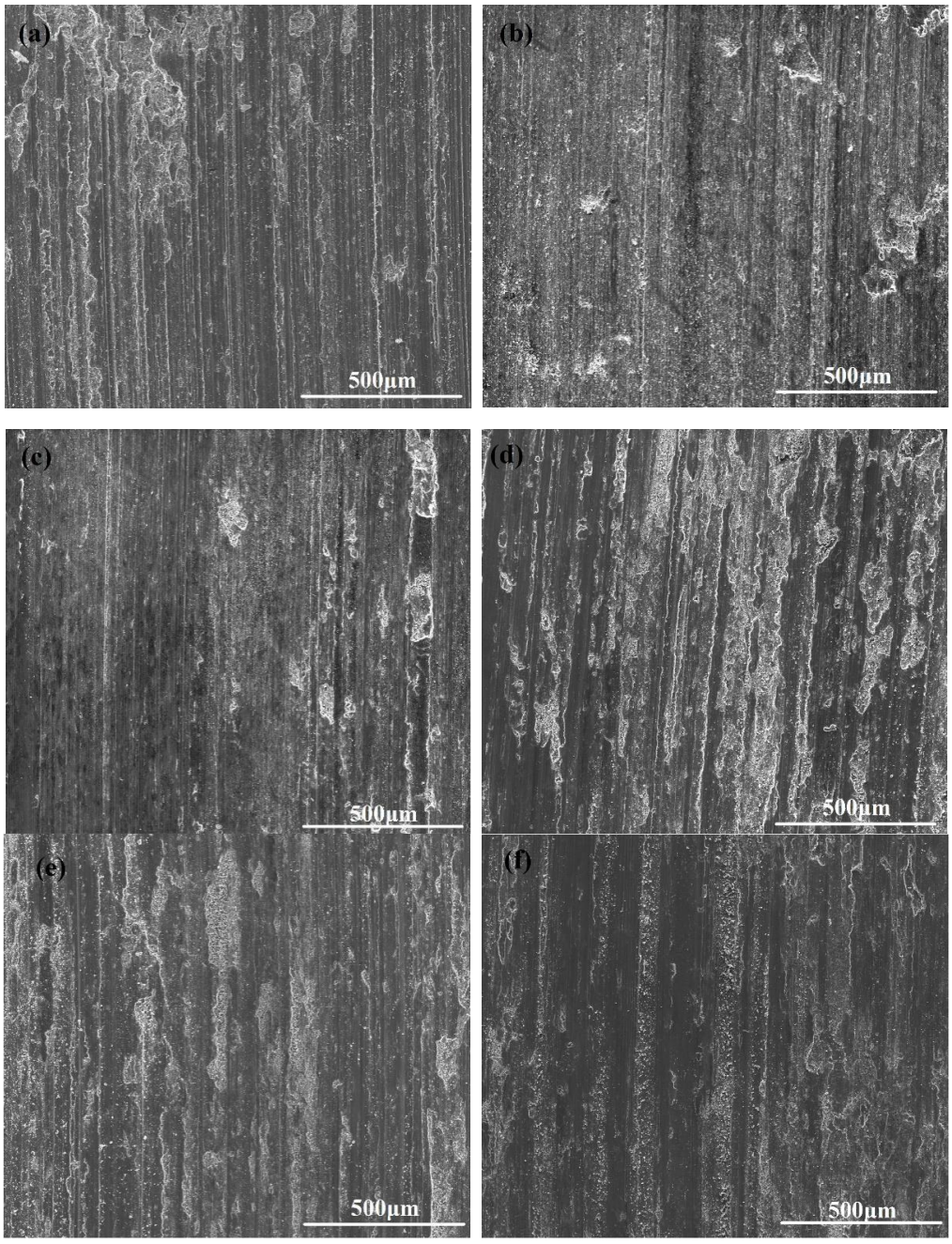

Figure 21. Wear morphology of rheoformed 2024 aluminum matrix composite component reinforced by Al_2O_3 nanoparticles with different volume fraction at 620 °C for 25 min stirring time (**a**) 0; (**b**) 1%; (**c**) 3%; (**d**) 5%; (**e**) 7%; (**f**) 10%.

4. Conclusions

(1) 2024 aluminum matrix composite components reinforced by Al_2O_3 nanoparticles were rheoformed successfully. Complete filling status and good surface quality were achieved in the rheoformed composite components. Microstructure at the top and middle side wall consisted of near spheroidal grains and liquid phase, indicating dependence of deformation on liquid incorporating solid grains (FLS) and sliding between solid grains (SSG). However, obvious elongated grains were noted in the low side wall and at bottom of the rheoformed composite components. It illustrated that deformation in these locations was dominated by plastic deformation of solid grains (PDS).

(2) Mechanical properties of the rheoformed composite components were influenced by stirring temperature, stirring time, and volume fraction of Al_2O_3 nanoparticles of composite semisolid slurries. The optimal UTS of 358 MPa and YS of 245 MPa were obtained at the bottom of the rheoformed composite components with 5% Al_2O_3 nanoparticles at 620 °C for 25 min stirring time. The increasing degrees of UTS are 17.5% and 31.7% as compared to the matrix component. Uniform dispersed Al_2O_3 nanoparticles and high density dislocations and dislocation tangles caused by PDS led to an improvement of mechanical properties. Needle-like Al_2CuMg phase and short-rod-like Al_2Cu phase were found in the microstructure of the rheoformed composite components due to natural ageing. $MgAl_2O_4$ phase has no effect on mechanical properties due to good wetting and high properties.

(3) T6 heat treatment led to an improvement of mechanical properties of the rheoformed composite components. UTS of 417MPa and YS of 328 MPa were achieved at bottom of the rheoformed composite components with 5% Al_2O_3 nanoparticles at 620 °C for 25 min stirring time. UTS, YS, and elongation of the composite components with T6 heat treatment were increased by 16.5%, 20.6%, and 5.6% respectively as compared to the composite component without T6 heat treatment. UTS and YS of the composite components with T6 heat treatment were increased by 36.7% and 49.1% respectively as compared to the matrix components with T6 heat treatment. Improvement of mechanical properties of the rheoformed composite components with T6 was attributed to a large amount of precipitated needle-like Al_2CuMg phase and short-rod-like Al_2Cu phase.

(4) Wear resistance of the rheoformed composite components increased as compared to that of the matrix component. Furthermore, wear resistance of the rheoformed composite components increased with an increase of Al_2O_3 nanoparticles from 1% to 7%. A slight decrease in wear rate of the rheoformed composite components resulted from 10% Al_2O_3 nanoparticles due to a decrease in effective dispersion of Al_2O_3 nanoparticles caused by greater agglomeration. The delamination and shallow ploughing grooves illustrate that the dominant wear mechanism was a combination mechanism of adhesion and delamination. To sum up, the optimal process parameters to obtain best comprehensive mechanical properties and resistance to wear are a stirring temperature of 620 °C, a stirring time of 25 min, and a volume fraction of 5% nano-sized Al_2O_3 nanoparticles.

Author Contributions: J.J. designed most experiments, analyzed the results, and wrote this manuscript. G.X. and Y.L. performed most experiments. Y.W. helped analyze the experimental data and gave some constructive suggestions on this manuscript.

Funding: This research was funded by the Natural Science Foundation of China (NSFC) under Grant No. 51375112.

Conflicts of Interest: The authors declare no conflicts of interest.

References

1. Mandal, D.; Viswanathan, S. Effect of heat treatment on microstructure and interface of SiC particle reinforced 2124 Al matrix composite. *Mater. Charact.* **2013**, *85*, 73–81. [CrossRef]
2. Mindivan, H.; Kayali, E.S.; Cimenoglu, H. Tribological behavior of squeeze cast aluminum matrix composites. *Wear* **2008**, *265*, 645–654. [CrossRef]

3. Bharath, V.; Nagaral, M.; Auradi, V.; Kori, S.A. Preparation of 6061Al-Al_2O_3 MMC's by stir casting and evaluation of mechanical and wear properties. *Procedia Mater. Sci.* **2014**, *6*, 1658–1667. [CrossRef]
4. Natarajan, N.; Vijayarangan, S.; Rajendran, I. Wear behaviour of A356/25SiC_p aluminium matrix composites sliding against automobile friction material. *Wear* **2006**, *261*, 812–822. [CrossRef]
5. Prabu, S.B.; Karunamoorthy, L.; Kathiresan, S.; Mohan, B. Influence of stirring speed and stirring time on distribution of particles in cast metal matrix composite. *J. Mater. Process. Technol.* **2006**, *171*, 268–273. [CrossRef]
6. Tjong, S.C.; Ma, Z.Y. High-temperature creep behaviour of powder-metallurgy aluminium composites reinforced with SiC particles of various sizes. *Compos. Sci. Technol.* **1999**, *59*, 1117–1125. [CrossRef]
7. Bajpai, G.; Purohit, R.; Rana, R.S.; Rajpurohit, S.S.; Rana, A. Investigation and testing of mechanical properties of Al-nano SiC composites through cold isostatic compaction process. *Mater. Today Proc.* **2017**, *4*, 2723–2732. [CrossRef]
8. Tatar, C.; Özdemir, N. Investigation of thermal conductivity and microstructure of the α-Al_2O_3 particulate reinforced aluminum composites (Al/Al_2O_3-MMC) by powder metallurgy method. *Phys. B Condensed Matter* **2010**, *405*, 896–899. [CrossRef]
9. Zhang, Q.; Wu, G.H.; Chen, G.Q.; Jiang, L.T.; Luan, B.F. The thermal expansion and mechanical properties of high reinforcement content SiCp/Al composites fabricated by squeeze casting technology. *Compos. Part A-Appl. S.* **2003**, *34*, 1023–1027. [CrossRef]
10. Chou, S.N.; Huang, J.L.; Lii, D.F.; Lu, H.H. The mechanical properties of Al_2O_3/aluminum alloy A356 composite manufactured by squeeze casting. *J. Alloy. Compd.* **2006**, *419*, 98–102. [CrossRef]
11. Chen, W.P.; Liu, Y.X.; Yang, C.; Zhu, D.Z.; Li, Y.Y. (SiCp + Ti)/7075Al hybrid composites with high strength and large plasticity fabricated by squeeze casting. *Mater. Sci. Eng. A* **2014**, *609*, 250–254. [CrossRef]
12. Wang, L.; Qiu, F.; Zou, Q.; Yang, D.L.; Tang, J.; Gao, Y.Y.; Li, Q.; Han, X.; Shu, S.L.; Chang, F.; et al. Microstructures and tensile properties of nano-sized SiC_p/Al-Cu composites fabricated by semisolid stirring assisted with hot extrusion. *Mater. Charact.* **2017**, *131*, 195–200. [CrossRef]
13. Guan, L.N.; Geng, L.; Zhang, H.W.; Huang, L.J. Effects of stirring parameters on microstructure and tensile properties of (ABO_w + SiC_p)/6061Al composites fabricated by semi-solid stirring technique. *Trans. Nonferrous Met. Soc. China* **2011**, *21*, s274–s279. [CrossRef]
14. Sameer, K.D.; Sumanm, K.N.S.; Tara, S.C.; Ravindra, K.; Palash, P.; Venkata, S.S.B. Microstructure, mechanical response and fractography of AZ91E/Al_2O_3 (p) nano composite fabricated by semi solid stir casting method. *J. Magn. Alloys* **2017**, *5*, 48–55.
15. Prashanth, K.G.; Scudino, S.; Chaubey, A.K.; Löber, L.; Wang, P.; Attar, H.; Schimansky, F.P.; Pyczak, F.; Eckert, J. Processing of Al–12Si–TNM composites by selective laser melting and evaluation of compressive and wear properties. *J. Mater. Res.* **2016**, *31*, 55–65. [CrossRef]
16. Prashantha, K.G.; Shahabia, H.S.; Attara, H.; Srivastavac, V.C.; Ellendtd, N.; Uhlenwinkeld, V.; Eckerta, J.; Scudino, S. Production of high strength $Al_{85}Nd_8Ni_5Co_2$alloy by selective laser melting. *Addit. Manuf.* **2015**, *6*, 1–5. [CrossRef]
17. Attar, H.; Bönisch, M.; Calin, M.; Zhang, L.C.; Scudino, S.; Eckert, J. Selective laser melting of in situ titanium—Titanium boride composites: Processing, microstructure and mechanical properties. *Acta Mater.* **2014**, *76*, 13–22. [CrossRef]
18. Cui, Y.N.; Wang, L.F.; Ren, J.Y. Multi-functional SiC/Al Composites for aerospace applications. *Chin. J. Aeronaut.* **2008**, *21*, 578–584.
19. Lee, S.S.; Yeo, J.S.; Hong, S.H.; Yoon, D.J.; Na, K.H. The fabrication process and mechanical properties of SiCp/Al-Si metal matrix composites for automobile air-conditioner compressor piston. *J. Mater. Process. Technol.* **2001**, *113*, 202–208. [CrossRef]
20. Koli, D.K.; Agnihotri, G.; Purohit, R. A review on properties, behaviour and processing methods for Al-nano Al_2O_3 composites. *Procedia Mater. Sci.* **2014**, *6*, 567–589. [CrossRef]
21. Raju, P.R.M.; Siriyala, R.; Raju, K.S.; Raju, R.V.R. Evaluation of fatigue life of Al2024/Al_2O_3 particulate nano composite fabricated using stir casting technique. *Mater. Today Proc.* **2017**, *4*, 3188–3196. [CrossRef]
22. Raturi, A.; Mer, K.K.S.; Pant, P.K. Synthesis and characterization of mechanical, tribological and micro structural behaviour of Al 7075 matrix reinforced with nano Al_2O_3 particles. *Mater. Today Proc.* **2017**, *4*, 2645–2658. [CrossRef]

23. Sajjadi, S.A.; Parizi, M.T.; Ezatpour, H.R.; Sedghi, A. Fabrication of A356 composite reinforced with micro and nano Al_2O_3 particles by a developed compocasting method and study of its properties. *J. Alloy. Compd.* **2012**, *511*, 226–231. [CrossRef]
24. Akbari, M.K.; Baharvandi, H.R.; Mirzaee, O. Fabrication of nano-sized Al_2O_3 reinforced casting aluminum composite focusing on preparation process of reinforcement powders and evaluation of its properties. *Compos. Part B-Eng.* **2013**, *55*, 426–432. [CrossRef]
25. Akbari, M.K.; Baharvandi, H.R.; Mirzaee, O. Nano-sized aluminum oxide reinforced commercial casting A356 alloy matrix: Evaluation of hardness, wear resistance and compressive strength focusing on particle distribution in aluminum matrix. *Compos. Part B-Eng.* **2013**, *52*, 262–268. [CrossRef]
26. Yang, Y.; Lan, J.; Li, X.C. Study on bulk aluminum matrix nano-composite fabricated by ultrasonic dispersion of nano-sized SiC particles in molten aluminum alloy. *Mater. Sci. Eng. A* **2004**, *380*, 378–383. [CrossRef]
27. Kandemir, S.; Atkinson, H.V.; Weston, D.P.; Hainsworth, S.V. Thixoforming of A356/SiC and A356/TiB_2 nanocomposites fabricated by a combination of green compact nanoparticle incorporation and ultrasonic treatment of the melted compact. *Metall. Mater. Trans. A* **2014**, *45*, 5782–5798. [CrossRef]
28. Jiang, J.F.; Wang, Y. Microstructure and mechanical properties of the rheoformed cylindrical part of 7075 aluminum matrix composite reinforced with nano-sized SiC particles. *Mater. Des.* **2015**, *79*, 32–41. [CrossRef]
29. Kandemir, S. Microstructure and mechonicol properties of A357/SiC nonocomposites fobricated by ultrosonic covitotion-based dispersion of ball-milled nonoparticles. *J. Compo. Mater.* **2017**, *51*, 395–404. [CrossRef]
30. ASTM Standard E8M. *Standard Test Methods for Tension Testing of Metallic Materials [Metric]*; ASTM International: West Conshohocken, PA, USA, 2008.
31. Chen, C.P.; Tsao, C.-Y.A. Semi-solid deformation of non-dendrtic structure-I. Phemonological behavior. *Acta Mater.* **1997**, *45*, 1955–1968. [CrossRef]
32. Kubotak, K.; Mabuchi, M.; Higashi, K. Review processing and mechanical properties of fine-grained Mg alloys. *J. Mater. Sci.* **1999**, *34*, 2255–2262. [CrossRef]
33. Sajjadi, S.A.; Ezatpour, H.R.; Beygi, H. Microstructure and mechanical properties of Al-Al_2O_3 micro and nanocomposites fabricated by stir casting. *Mater. Sci. Eng. A* **2011**, *528*, 8765–8771. [CrossRef]
34. Yar, A.A.; Montazerian, M.; Abdizadeh, H.; Baharvandi, H.R. Microstructure and mechanical properties of aluminum alloy matrix composite reinforced with nano-particle MgO. *J. Alloy. Compd.* **2009**, *484*, 400–404. [CrossRef]
35. Nguyen, Q.B.; Gupta, M. Enhancing compressive response of AZ31B using nano-Al_2O_3 and copper additions. *J. Alloy. Compd.* **2010**, *490*, 382–387. [CrossRef]
36. Sastry, S.; Krishnab, M.; Uchil, J. A study on damping behaviour of aluminite particulate reinforced ZA-27 alloy metal matrix composites. *J. Alloy. Compd.* **2001**, *314*, 268–274. [CrossRef]
37. Su, H.; Gao, W.L.; Feng, Z.H.; Lu, Z. Processing, microstructure and tensile properties of nano-sized Al_2O_3 particle reinforced aluminum matrix composites. *Mater. Des.* **2012**, *36*, 590–596. [CrossRef]
38. Zhong, X.L.; Wong, W.L.E.; Gupta, M. Enhancing strength and ductility of magnesium by integrating it with aluminum nanoparticles. *Acta Mater.* **2007**, *55*, 6338–6344. [CrossRef]
39. Ghidelli, M.; Sebastiani, M.; Collet, C.; Guillemet, R. Determination of the elasticmoduli and residual stresses of freestanding Au-TiW bilayer thin films by nanoindentation. *Mater. Des.* **2016**, *106*, 436–445. [CrossRef]
40. Ghidelli, M.; Sebastiani, M.; Johanns, K.E.; Pharr, G.M. Effects of indenter angle on micro-scale fracture toughness measurement by pillar splitting. *J. Am. Ceram. Soc.* **2017**, *100*, 5731–5738. [CrossRef]
41. Mazahery, A.; Abdizadeh, H.; Baharvandi, H.R. Development of high-performance A356/nano-Al_2O_3 composites. *Mater. Sci. Eng. A* **2009**, *518*, 61–64. [CrossRef]
42. Lan, J.; Yang, Y.; Li, X.C. Microstructure and microhardness of SiC nanoparticles reinforced magnesium composites fabricated by ultrasonic method. *Mater. Sci. Eng. A* **2004**, *386*, 284–290. [CrossRef]
43. Korgul, P.; Wilson, D.R.; Lee, W.E. Microstructural analysis of corroded alumina-spine1 castable refractories. *J. Eur. Ceram. Soc.* **1997**, *17*, 77–84. [CrossRef]
44. Ghosha, A.; Sarkar, R.; Mukerjee, B.; Das, S.K. Effect of spinel content on the properties of magnesia-spinel composite refractory. *J. Eur. Ceram. Soc.* **2004**, *24*, 2079–2085. [CrossRef]
45. Zang, J. Wetting and Adhesion at Al/MgAl2O4 Interface and the Effect of Substrate Crystallographic Orientation. Ph.D. Thesis, Jilin University, Changchun, China, 2014.

46. Alhawari, K.S.; Omar, M.Z.; Ghazali, M.J.; Salleh, M.S.; Mohammed, M.N. Wear properties of A356/Al_2O_3 metal matrix composites produced by semisolid processing. *Procedia Eng.* **2013**, *68*, 186–192. [CrossRef]
47. Ehtemam-Haghighi, S.; Prashanthb, K.G.; Attar, H.; Chaubey, A.K.; Caod, G.H.; Zhang, L.C. Evaluation of mechanical and wear properties of Ti-xNb-7Fe alloys designed for biomedical applications. *Mater. Des.* **2016**, *111*, 592–599. [CrossRef]